Original Paper

Eletrônica de Potência
Open Journal of Power Electronics

Received June 02, 2025; accepted September 24, 2025; Date of publication October 22, 2025.
The review of this paper was arranged by Associate Editor Wilmar P. Castiblanco and Editor-in-Chief Heverton A. Pereira.

Digital Object Identifier http://doi.org/10.18618/REP.e202554

Induction Motor Fault Diagnosis Based on the Machine Temperature, Vibration Analysis and Sensors Fusion

Daniel P. Sifuentes Filho[1], Ygor F. Ginu[1], Khristian M. de Andrade Jr.[1,*], Bernardo P. de Alvarenga[1], Geyverson T. de Paula[1]

[1]Federal University of Goiás, School of Electrical, Mechanical and Computer Engineering, Goiânia, 74605-010, Brazil.

e-mail: daniel_sfilho@hotmail.com;ygorferreiraginu@gmail.com; khristian@discente.ufg.br*; bernardo_alvarenga@ufg.br; geyverson@ufg.br.
*Corresponding author.

ABSTRACT The most common motor used for industrial, residential and commercial applications is the induction motor (three or single phase). This motor is very reliable, but faults still may occur. The present paper focuses on the diagnosis of induction motor faults based on its temperature and vibration behaviors on steady-state operation. The proposed method is based on the Extended Park Transform, enabling sensor fusion which reduces the amount of data required for fault identification to 1/3 and allows the usage of a shallow artificial neural network. To validate the proposed method, experiments have been carried using a single phase induction motor operating under normal and fault conditions (short-circuit between main winding turns, auxiliary turns, main-auxiliary windings and with contaminated bearing lubrication). The results proves the efficacy of the proposed method, which has reached an accuracy over 99.5% in the process of fault identification using low cost sensors/equipment.

KEYWORDS Single Phase Induction Motor, Fault Diagnosis, Low Cost, Artificial Neural Network

I. INTRODUCTION

Induction motors are used in the most variety of applications (electrical vehicles, industrial, commercial or residential applications) due to their low cost, reliability, robustness and high efficiency [1]–[3]. These motors represent a great percentage of the power consumption in developed countries [4], showing the great importance that they have in the production process. As mentioned, they are very reliable, although still susceptible to faults due to ageing or even overload conditions. These faults can result in great damage to the industrial process, causing production losses, thus their quick identification, diagnosis and repair is very important and object of many researches around the world [5]–[12].

Since faults in induction machines may result in loss of production, the maintenance sector is vital to prevent these faults or fix them once they occur [13]–[15]. The researches on this topic are constantly under development by many researchers and companies. The predictive maintenance considers continuous monitoring of the machine to predict when it is going to fault. This type of maintenance may be costly, but reduces the amount of interventions and process downtime.

According to the surveys carried out by many researches, papers and even surveys conducted by IEEE and EPRI (Electric Power Research Institute) [16]–[20], faults in induction motors mostly occur in the bearings (45-50%), followed by winding faults (35-45%) and rotor faults (10%, approximately).

Non-intrusive techniques that permit quick fault identification in electrical machines are the main focus of all researches since it is possible to evaluate any machine that is already operating. Within the various non-intrusive techniques, two of them can be employed with low-cost sensors but with good accuracy. These two techniques are the temperature and vibration monitoring. These tools are suitable for fault identification in induction motors since most faults cause temperature and vibration rising [7], [21].

Temperature monitoring with non-intrusive sensors alone is insufficient for precise fault identification in induction machines because faults like winding short circuits or bearing issues cause similar temperature rises. However, combining temperature data with other non-intrusive methods, such as vibration analysis, can enhance fault diagnosis when used as a weighting factor in systems like Artificial Neural Networks, Fuzzy Logic, Deep Learning, or decision trees.

Vibration analysis using a 3 DoF accelerometer is a widely researched, non-intrusive method attractive to industry. Key challenges include implementing low-cost yet accurate sensors, developing sensorless vibration prediction, identifying single and multiple faults from vibration patterns, and reducing input data to lower computational effort and enable fast fault detection.

When the vibration sensors are placed on the bearing cap, the rotor eccentricities, bearing faults, bent shaft and other rotor related fault can be easily identified. On the other hand, when the sensors are placed on the stator the fault

identification process can also identify winding faults, phase unbalance and etc [16], [21], [22].

Online fault diagnosis is increasingly important in the context of IoT and Industry 4.0. It requires local data collection and cloud-based systems (local or remote) with powerful computing to quickly process large data volumes. Non-intrusive, low-cost sensors can be deployed on all motors in an industrial plant to predict and prevent failures. However, more sensors generate more data traffic, making it essential to reduce the amount of data collected and transmitted.

This paper presents a new method for fault identification in induction motors that reduces the number of input variables to minimize data traffic and computational effort, while maintaining accuracy. The approach uses sensor fusion based on the Extended Park Transform (dqx) combined with temperature monitoring, processed by an Artificial Neural Network (ANN).

Experimental tests were conducted on a 1/4 hp single-phase induction motor, collecting temperature data from three sensors and vibration data from a low-cost 3 DoF accelerometer. Various motor conditions were tested, including healthy operation, winding short-circuits, and bearing faults. A thermographic camera was used to calibrate temperature measurements. Although tested on a single-phase motor, the method can be adapted to other machines by retraining the ANN. The main goal is to reduce transmitted sensor data while preserving high fault detection accuracy.

II. FAULT TYPES, TEMPERATURE AND FREQUENCY SPECTRUM

The faults in electrical machines can be divided in two main types: electrical and mechanical. A mechanical fault may not necessarily lead to an electrical fault, although it can be sensed in the windings (flux-linkage, induced voltage, induced and phase currents) or by means of the temperature rising around the failure. Examples of mechanical faults are rotor eccentricity, bent shaft and bearing faults. Yet, an electrical fault, according to its gravity, leads to a temperature rising, mechanical failure or, at least, reinforce an existing failure and cause unbalance, vibration and, consequently, wear and tear in the bearings and bearings cap.

As mentioned, the faults in the bearings are the most common faults in electrical machines, corresponding to 50% of all faults, approximately. This type of faults can be sensed during the vibration analysis at frequencies dependent on the bearing geometry and bearing and motor running speed [17], [20], [21]. Eccentricities or unbalances in the rotor causes high intensity vibrations along the radial directions with frequency equal to the shaft rotating one. The presence of this fault can be noticed via the vibration analysis when a peak at the shaft rotating frequency is present [17], [21]. Now, if the rotor is bent, the frequencies equal to one, two and three times the rotating frequency, with amplitudes in descending order, indicates the presence of such fault [20].

When it comes to electrical faults in induction motors, which corresponds to 45% of all faults, approximately, they can be divided in stator and rotor faults. Examples of stator faults are phase-to-phase fault or phase unbalance in three phase motors, phase-to-earth fault or inter-turn fault for both three and single phase motors and main winding to auxiliary winding, auxiliary winding to auxiliary winding or capacitor failure (short-circuited or open-circuited) for single phase motors. Broken bars or broken end-ring are examples of rotor faults in squirrel-cage rotors, whereas inter-turn faults are examples of faults in wound-rotors.

Inter-turn short-circuits in the main or auxiliary windings of single phase motors or auxlliary-main winding short-circuit represent a condition similar to that caused by unbalanced phase currents in three phase motors. This is due to the resulting unbalance distribution of electromagnetic forces. Substantial spectrum around twice the supply frequency ($2 \times f_S$) and around the rotating speed frequency (f_ω) and its multiples indicate the presence of these faults [20]. Moreover, other harmonics can also be noticed depending on the machine topology (three phase, single phase, poles number) and winding distribution.

Another example of how a fault can affect the vibration and how can be detected is related to the broken bars fault in squirrel-cage rotors. This fault affects negatively the rotating field created by the rotor, thus resulting in unbalanced distribution of electromagnetic forces. This fault can be detected when the vibration frequency spectra presents reasonable component values at one and two times the rotating speed frequency ($1 \times f_\omega$, $2 \times f_\omega$) and frequencies around the rotor-bar passing frequency [20].

III. PROPOSED METHOD AND THE FAULT IDENTIFICATION SYSTEM

The proposed method is suitable for 3 DoF vibration sensors (accelerometer) placed on the surface of the stator with one of its axis aligned with the rotor shaft as will be shown in the experimental setup.

The proposed method, referred here as to Extended Vibration Vector (EVV), is based on the Extended Park Transform (dqx) [23], [24]. This way, it is possible to perform a vibration sensors fusion since they are already in an orthogonal coordinate system and look into only one resultant vibration signal (Extended Vibration Vector) that carries the information of the machine condition. This resultant vector will have its amplitude and phase angle changed according to the vibration present in the X, Y and/or Z coordinates.

This sensor fusion technique will allow the reduction of input data as well as the reduction of data transferred through the connection to the online Fault Identification System.

The basis of the dqx Transform has been developed for balanced systems only, this way, in the proposed EVV, a consideration must be followed: one of the accelerometers axis must be neglected. The neglected axis must have a lower contribution on fault identification process, i.e., must carry

no substantial information related to the desired fault type. Otherwise, the fault identification process may fail.

Considering the background of numerous research in literature and the state of art, as in [5]–[21], the most suitable axis to be neglected is the axial machine's axis since monitoring this axis vibration is specially relevant for bearing faults type and does not contain a remarkable harmonic content related to winding faults or rotor faults.

Bearing in mind the aforementioned considerations, the sensor fusion is performed by means of (1):

$$\begin{bmatrix} V_0 \\ V_R \end{bmatrix} = \begin{bmatrix} \cos(\theta_v) & \sin(\theta_v) \\ -\sin(\theta_v) & \cos(\theta_v) \end{bmatrix} \begin{bmatrix} V_A \\ V_B \end{bmatrix} \tag{1}$$

where V_A and V_B are the two selected vibration axis that are orthogonal to each other; V_R is the resultant EVV and is equal to $\sqrt{V_A^2 + V_B^2}$; V_0 will always be zero; and θ_v is the vibration resultant orientation, i.e., where the EVV is pointing in the plane formed by V_A and V_B as expressed in (2) and illustrated in Fig. 1.

$$\theta_v = \tan^{-1}\left(\frac{-V_A}{V_B}\right) \tag{2}$$

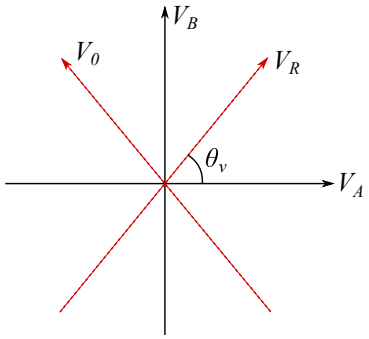

FIGURE 1. EVV coordinates

This is equivalent to aligning the transformation axis with the instantaneous vector in the original V_A-V_B plane, similarly to the classical Park Transform but with a time-varying angle defined by the measured signals themselves rather than by a rotor or synchronous reference frame. According to the expression for θ_v, this angle corresponds to the angle between the vibration vectors V_A and V_R , as illustrated in Fig. 1. As the transformation is performed using , the V_0 value will always be zero as an intrinsic property of this transformation as well as in the extended park transformation [23], [24].

The frequencies present in V_A and V_B signals will not be lost or even affected by the transformation, but they will be merged according to θ_v. Thus, the frequency spectrum of V_R will be different from V_A and V_B spectrum, having an average value and accounting for all frequencies present in V_A and V_B. To support this, consider a complex signal $S(t)$ defined as (3) in the time domain t.

$$S(t) = V_B(t) - jV_A(t) = \sum_k s_k e^{j\omega_k t} \tag{3}$$

where s_k and ω_k are complex coefficients for phase and amplitude of V_A and V_B.

Now, V_R^2 can be computed by means of (4).

$$V_R^2(t) = V_A^2(t) + V_B^2(t) = S(t)S^*(t) \tag{4}$$

in which $S^*(t)$ is the complex conjugate of $S(t)$.

Finally, V_R can be rewritten as shown in (5).

$$V_R = \left(\sum_k s_k e^{j\omega_k t}\right)\left(\sum_m s_m^* e^{-j\omega_m t}\right)$$

$$V_R = \sum_k \sum_m s_k s_m^* e^{j(\omega_k - \omega_m)t} \tag{5}$$

From (5), it is clear that $V_R(t)$ contain DC terms ($k = m$), proportional to the energy of each spectral line $|s_k|^2$, which never cancels. Also, it contains AC terms ($k \neq m$) with components at frequencies $|\omega_k - \omega_m|$.

Because the modulus operation is nonlinear, $V_R(t)$ also contains harmonics and sum-frequency components derived from these terms. Therefore, identical frequency components present in both V_A and V_B do not cancel out globally; their energy is preserved in the DC and AC terms of $V_R^2(t)$, and remains present in $V_R(t)$.

Furthermore, the mean (DC) component of $V_R(t)$, i.e., $|s_k|^2$ reflects the total vibrational energy level captured by both V_A and V_B. So the mean power of V_R corresponds to the sum of the powers of all spectral lines from both channels. This is a compact indicator of steady mechanical offsets, continuous unbalance, preload, or constant-contact rubbing. Removing the mean value (DC) would discard valuable diagnostic information.

In practice, the mean value (DC) is estimated over time windows covering multiple machine cycles (or via recursive averaging with a forgetting factor) after removing sensor bias. Subsequently, $\overline{V_R^2}$ is computed (implicitly) as a direct measure of mean vibrational power. Including these quantities as part of the feature set improved ANN classification accuracy in our experiments.

The next step consists of submiting V_R to a bandpass filter and select the harmonic components that contribute substantially to the identification process. This step will be further detailed in the results and discussion section since it will be based on empirical results. It is certain that the mean value must be preserved, as it is another characteristic of V_R.

After the filtering process, the filtered signal, referred here as to V_R^*, must be submitted to a Discrete-Fourier Transform (DFT), converting it from time-domain to frequency-domain. The main harmonic orders will be submitted to the ANN along with the temperature signal. It is worth mentioning that the temperature monitoring has the purpose of being a weighting factor for fault identification.

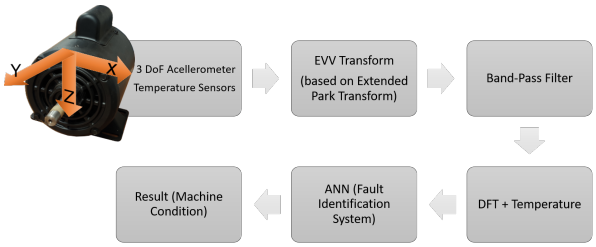

FIGURE 2. Proposed method flowchart.

The usage of one or more temperature sensors and where they should be placed in the motor will be discussed and evaluated in the results and discussions section.

The flowchart that summarizes the proposed method is found in Fig. 2.

IV. TEST BENCH AND EXPERIMENTAL PROCEDURE

The test bench, the sensors (temperature and acellerometer) and the proposed experimental procedure are detailed in this section. To validate the proposed method, several tests have been performed on a single-phase induction motor under healthy condition and multi-faulty conditions. This motor has its parameters detailed in Table 1.

TABLE 1. Machine Parameters

Parameter	Value
Power [kW (HP)]	0.18 (0.25)
Pole number	4
Frequency [Hz]	60
Rated voltage [V]	127/220
Rated current [A]	6.75/2.90
Startup current [A]	30.4/13.1
Rated speed [rpm]	1750
Rated slip [%]	2.78

A data acquisition system has been used with four NTC sensors for monitoring the motor and environment temperature behavior. The data acquisition system consists of an ATmega328 micro controller, attached to an Arduino Nano card transmitting the temperature measurement data via serial. The data collections are then treated and plotted in graphic format according to scheduled time intervals.

Temperature sensors (NTC) have been attached to three strategic points in the body of the motor (Tc1, Tc2 and Tc3). Tc1 is attached to the enclosure, whereas Tc2 to the frontal bearing and Tc3 to the end bracket. Another sensor has been responsible for measuring the environment temperature (Tc4) in order to calibrate the temperature measured by the other three sensors. See Fig. 3. For comparison purposes, thermographic monitoring has been carried out with a thermographic camera CIR FLIR SYSTEMS ®.

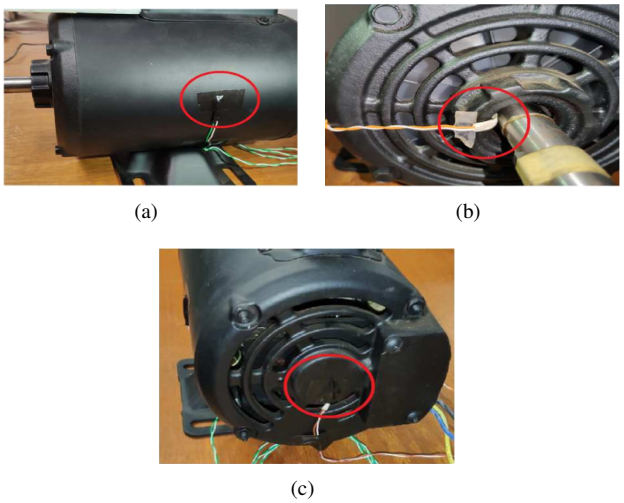

FIGURE 3. Thermocouples allocation. (a) Tc1 (b) Tc2 (c) Tc3.

A low-cost 3 DoF accelerometer MPU6050 has been used for vibration data collection. Its range is $\pm$2g, $\pm$4g, $\pm$8g and $\pm$16g and it has been placed on top of the motor's stator as illustrated in Fig. 4 as well as the sensor coordinates. The vibration data is collected, applied to EVV for sensor fusion and then transmitted to a PC where the Fault Identification System based on ANN will filter, process the data and classify the current situation according to the previously trained/learned conditions.

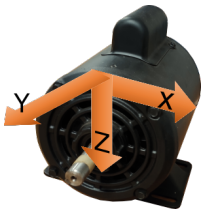

FIGURE 4. Sensor placed on stator and its coordinates.

An experimental bench has been assembled, as illustrated in Fig. 5. It is equipped with an emergency button for safety reasons during short-circuit conditions. The load machine is a Permanent Magnet Synchronous Generator (PMSG) connected to a resistive load.

First, for future data comparison and to train the ANN, a healthy motor operating under four different load conditions has been tested: no-load; 50%; 80% and 100% of the rated power.

During short-circuit tests, an intermittent operating condition has been emulated. The intention is to reproduce the functioning of machines that operate in a sequence of identical cycles. These cycles are equivalent to startup, a period of operation with constant load and a standby period. For the contaminated bearing lubrication test, the motor has been also operated and tested under four different load conditions: no-load; 50%; 80% and 100% of the rated power.

Although the intermittent operating condition has been considered and the vibration and temperature data has been logged during all the experiment, only the data acquired in steady state operating condition has been used to train the ANN. Therefore, this paper does not deal with fault identification during transient/non-stationary conditions.

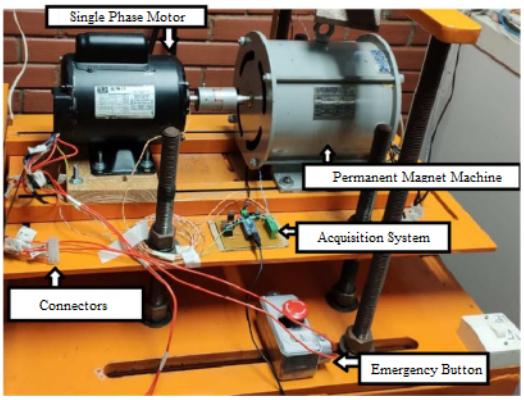

FIGURE 5. Experimental bench

A. SHORT-CIRCUIT TESTS

The most common types of short-circuit in single phase induction motor have been tested. The distribution of single phase induction motor's windings and the points available for short-circuit tripping can be seen in the schematic diagram illustrated in Fig. 6.

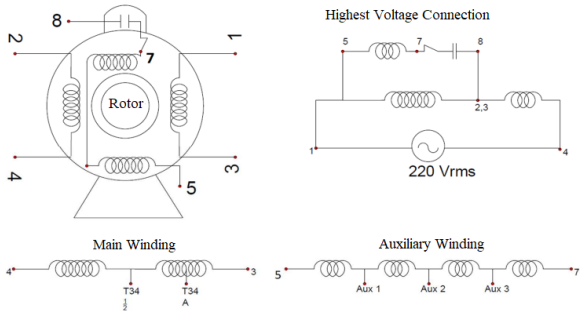

FIGURE 6. Schematic diagram of the motor auxiliary and main windings

The emulated short-circuits conditions and the points of the winding turns connected are listed below:

1) Turn-to-turn short-circuit in the auxiliary winding (Aux-Aux Fault): connections between the Aux 1, Aux 2 and Aux 3 points available along the auxiliary winding.
2) Short-circuit between auxiliary and main windings (Aux-Main Fault): connections were made between points 2, Aux 1, Aux 2 and Aux 3 along the main and auxiliary windings.
3) Turn-to-turn short-circuit in the main winding (Main-Main Fault): connections have been made between points T34 A and T34 $1/2$ available along the main winding.

B. CONTAMINATED BEARING LUBRICATION TEST

Experiments have been carried out to emulate the condition of contaminated bearing lubrication (Bearing Fault). The entrance of foreign bodies in the bearing is possible due to damage in the bearing shield/seal. This damage is caused by impact or loosening during long working terms. In this article, the bearing shield/seal has been broken and the lubrication has been contaminated with thin sand grains. This emulates the situation of contamination by dirt particles present in industrial environment (Fig. 7), increasing the friction torque and the vibration. In order to measure and understand the level of contamination, the temperature characteristic of the motor operating coupled to the load and under normal conditions and with contaminated and non contaminated bearing have been acquired and compared. This way, it is possible to determine if the machine under investigation is occurred of bearing faults.

(a) (b)

FIGURE 7. Motor bearing. (a) Healthy bearing. (b) Contaminated bearing.

V. RESULTS AND DISCUSSIONS

This section presents the results obtained with the experiments and the discussions regarding the implementation of the proposed method.

The first point to be discussed is related to the constraint of the proposed method that uses only two of three accelerometers axis. As mentioned, the neglected axis must have no substantial contribution on fault identification as well as in the description of the machine vibration behavior. For the sensor coordinates considered in all tests performed during this research, as illustrated in Fig. 4, the accelerometer axis neglected is the Y-axis since the vibration collected in its direction is considerably lower, when compared to the X- and Z-axis, for the fault conditions tested. Maybe, for fault conditions different of those observed and tested in this research, the Y-axis may have a substantial information that must be considered.

To illustrate how Y-axis behaves during a fault condition and compare it to X- and Z-axis and justify why it has been neglected, the Fig. 8 shows the data collected for X-, Y- and Z-axis. For all fault conditions tested during this research, Y-axis vibration data presented a similar aspect of Fig. 8 when compared to X- an Z-axis, showing no relevant contribution for data analysis.

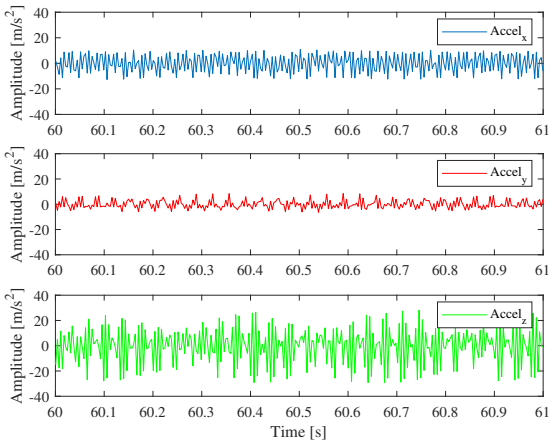

(a)

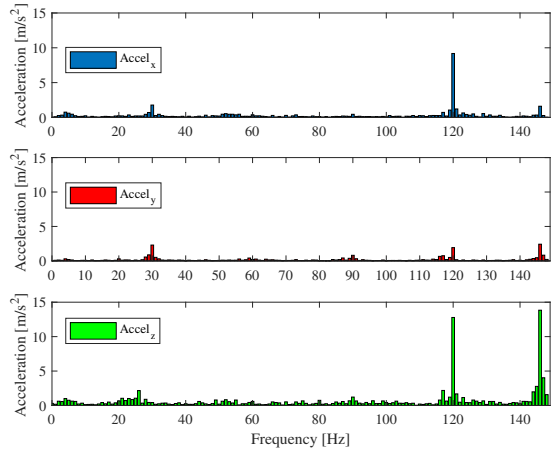

(b)

FIGURE 8. Comparison of X-, Y- and Z-axis vibration data under main-winding fault condition. (a) Time-domain data of X-, Y- and Z-axis. (b) Frequency spectrum of X-, Y- and Z-axis data.

Next, the selected X- and Z- vibration axis are applied to (1) and (2) in order to obtain the V_R, the resultant EVV. For sake of clarity, the X- and Z- vibration axis are V_A and V_B, respectively, in (1) and (2). It is found in Figs. 10 and 11, one result of V_R in its time-domain and frequency-domain, respectively, for each kind of fault considered in this paper. As can be noticed, all V_R have an average value and a different harmonic content due to the related fault. Therefore, it is possible to select the most important/relevant frequencies that will be applied to the ANN for fault identification.

To cover all interested faults, the selected frequencies are 0Hz (DC component of DFT), 17Hz, 21Hz, 29Hz, 46Hz, 120Hz and 140Hz. These frequencies are highlighted in Fig. 11 by the red vertical lines surrounding them. Furthermore, these frequencies have a relevant value that changes according to the fault and load condition.

The chosen frequencies will compose the input vector of the ANN along with the temperature acquired by each thermocouples (TC).

Since this paper is focused in low-cost systems as the MPU6050, the number of TCs and where they are placed is one of the interesting variable that is considered. This way, although four thermocouples have been used, the TC4 that acquires the environment temperature will be neglected in the fault identification process since this temperature will vary according to the place where the motor is installed and in the presented case it has been used to calibrate the system. With three TCs (Tc1,2,3), the input vector can be composed of the seven selected frequencies in addition to one, two or three temperature signals. Therefore, the resulting combination yields seven different input vector strategies to the fault identification system, as listed in Table 2. For comparison purpose, an additional input vector considering only the V_R^* has been tested.

TABLE 2. Input vectors

Input Vector	Vector Length
V_R^*	7
V_R^* + Tc1	8
V_R^* + Tc2	8
V_R^* + Tc3	8
V_R^* + Tc1,2,3	10
V_R^* + Tc1,2	9
V_R^* + Tc1,3	9
V_R^* + Tc2,3	9

Although the length of the input vector vary depending on the number of TCs considered, the core of the fault identification system is based on a shallow ANN with 1 hidden layer with 10 neurons, and the output of this system is as described in Table 3, being composed of 5 outputs that classify motor condition.

The choice of a shallow ANN lies on the fact that with the reduced number of input parameters there is no need for a deep ANN or deep learning tool as can be found in many other researches published [19], [25], [26]. This reduction in the number of input parameters has been achieved thanks to the proposed method which, firstly, reduced the 3 vectors into 2 vector, by neglecting the Y-axis contribution, then reduced the 2 remains vectors into 1 vector, namely V_R, and finally, reducing it to its main harmonic components, V_R^*.

If it is considered that X-, Y- and Z-axis have 151 harmonic components (from DC to 150Hz), and if they were reduced to their main harmonic components, which in most case will result in more than 7 components each one [27], it can be stated that the proposed method presented in this paper would result in a reduction of at least 2/3 of the input parameters. As a consequence, a shallow ANN can be used.

Another novelty that must be highlighted is that there is no need of evaluating a set of features or a set of statistical features (named: Mean value (μ); Standard deviation (σ); Skewness; Kurtosis; Mean squared value ($\overline{V_R^2}$); Mean bearing temperature, etc.) for the signals as employed in some

approaches presented in the literature [19], [28], [29]. The absence of this need makes the proprosed method simpler than others and, as will be further discussed, keeps high level of accuracy during the fault identification process.

All this process helps not only in the reduction of the input parameters and in the ANN hidden layer size, but also in reducing the computational effort needed to solve the problem.

Moreover, the reduction in the data transmitted from the local low-cost device (that contains the accelerometer and thermocouples) is achieved if this device can at least apply (1) and (2), which can be considered a very simple task for any embedded micro controller.

Therefore, in order to summarize the advantages of the proposed method, a short list is presented below.

- Compactness – combines two vibration channels and one temperature signal into a small, information-rich vector.
- Complementarity – time-domain statistics capture global behavior and impulsive events, while spectral amplitudes capture specific fault-related orders, and temperature adds operational context.
- Robustness – the combination increases resilience to noise, load changes, and transients.
- Generality – features are not machine-specific, enabling adaptation to other rotating machinery with minimal changes.
- Low computational cost – features are inexpensive to compute, enabling real-time deployment in embedded systems.

TABLE 3. ANN Classification Code

Condition	Code
Aux-Aux Fault	10000
Aux-Main Fault	01000
Main-Main Fault	00100
Bearing Fault	00010
Healthy Motor	00001

The training, validation and test procedures of the ANN have been carried out with a total of 728 samples (70% for training, 15% for validation and 15% for testing).

The accuracy of each trained ANN according to the input vectors is shown in Table 4. The corresponding confusion matrix can be depicted in Fig. 9.As can be noticed, if the input vector is composed only of V_R^*, a very high accuracy ratio can be achieved as well as the lowest cost system, since it will be comprised only of the 3 DoF accelerometer and the micro controller. On the other hand, if the temperature measurement of at least one thermocouple is taken into account, this accuracy increases and can achieve 100%.

The reason why the input vectors comprised of V_R^*+Tc2, V_R^*+Tc2,3 and V_R^*+Tc1,2,3 have achieved the highest precision is due to the difficulty of defining the motor condition

FIGURE 9. Confusion Matrix for the proposed ANN

when the only fault present in the motor is in the front bearing. As can be observed in Figs. 10 and 11, the contaminated bearing fault has a low overall contribution in the chosen frequencies and could cause the ANN to misunderstand it as a healthy motor under low load condition.

Therefore, if the contaminated bearing fault condition was tested for the end bracket, it could be stated that the Tc3 would have a greater importance as an input parameter for the fault identification system.

As a conclusion, the best combination for monitoring the motor condition is V_R^* + Tc2,3. This way, it would be possible to identify both, front bearing and end bracket failures as well as any one of the proposed winding faults (Aux-Aux Fault, Aux-Main Fault, Main-Main Fault).

TABLE 4. Results Accuracy

Input Vector	Accuracy
V_R^*	99.5 %
V_R^* + Tc1	99.7 %
V_R^* + Tc2	100 %
V_R^* + Tc3	99.8 %
V_R^* + Tc1,2,3	100 %
V_R^* + Tc1,2	99.8 %
V_R^* + Tc1,3	99.7 %
V_R^* + Tc2,3	100 %

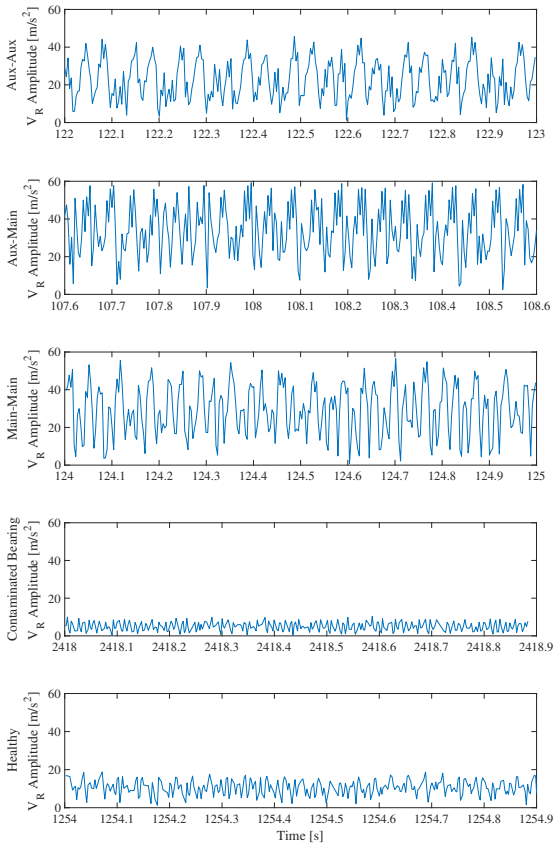

FIGURE 10. Time-domain V_R vector signal for each fault. From top to the bottom: Auxiliary-to-Auxiliary winding fault, Auxiliary-to-Main winding fault, Main-to-Main winding fault, Contaminated Bearing (no-load) and Healthy motor(Full load)

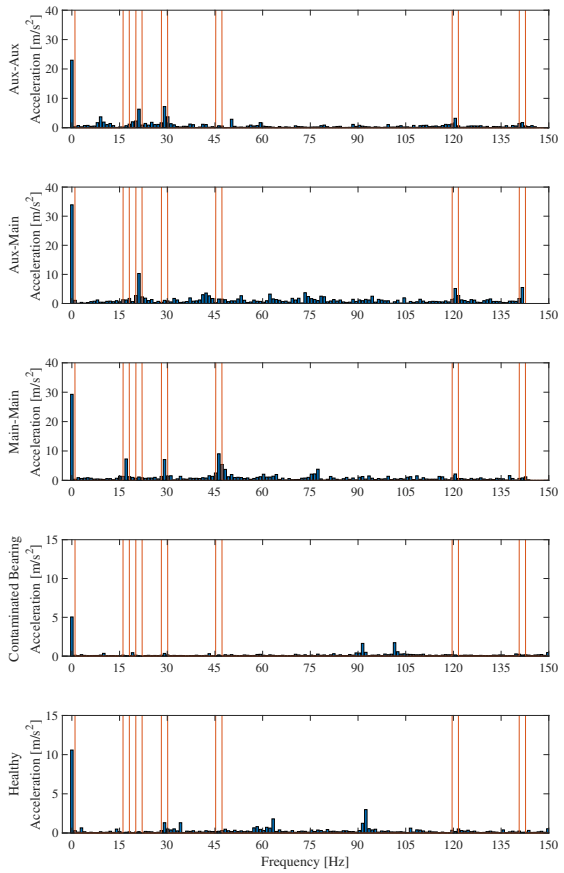

FIGURE 11. Frequency-domain V_R vector signal for each fault. From top to the bottom: Auxiliary-to-Auxiliary winding fault, Auxiliary-to-Main winding fault, Main-to-Main winding fault, Contaminated Bearing(no-load) and Healthy motor(Full load)

VI. CONCLUSION

Faults in induction motors may lead to severe losses in the industrial process. Thus, when a fault occurs, its quick identification and repair is vital. The present paper has proposed a method to identify the type of the faults considering the motor temperature and vibration analysis by means of a sensor fusion. This fusion is made by means of adapting the Extended Park Transform to this application, enabling the usage of a shallow artificial neural network. Several tests have been carried out in order to validate the method for a single-phase induction motor. The tests have proved the efficacy of the proposed method: it achieved an accuracy over 99.5% when identifying the type of the fault that the motor has been submitted. In addition, the sensors/equipment needed for the implementation of the method have low cost, showing the robustness of the proposed method.

ACKNOWLEDGMENT

All authors would like to thank CNPq, Coordenação de Aperfeiçoamento de Pessoal de Nível Superior - Brasil (CAPES) (Finance Code 001) and FAPEG (Fundação de Amparo à Pesquisa do Estado de Goiás) for funding guarantee and support.

AUTHOR'S CONTRIBUTIONS

D.P.S.FILHO: Data Curation, Formal Analysis, Investigation, Software. **Y.F.GINU:** Data Curation, Formal Analysis, Investigation, Software. **K.M.A.JUNIOR:** Writing – Original Draft, Writing – Review & Editing. **B.P.ALVARENGA:** Supervision. **G.T.PAULA:** Conceptualization, Formal Analysis, Methodology, Supervision, Validation.

PLAGIARISM POLICY

This article was submitted to the similarity system provided by Crossref and powered by iThenticate – Similarity Check.

DATA AVAILABILITY

The data used in this research is available in the body of the document.

REFERENCES

[1] Baoquan Kou, Liyi Li, Shukang Cheng, Fanrong Meng, "Operating control of efficiently generating induction motor for driving hybrid electric vehicle", *IEEE Transactions on Magnetics*, vol. 41, no. 1, pp. 488–491, 2005, doi:10.1109/TMAG.2004.838980.

[2] A. T. de Almeida, F. J. T. E. Ferreira, G. Baoming, "Beyond Induction Motors—Technology Trends to Move Up Efficiency", *IEEE Transactions on Industry Applications*, vol. 50, no. 3, pp. 2103–2114, 2014, doi:10.1109/TIA.2013.2288425.

[3] A. Gonzalez, C. Hernandez, M. A. Arjona, "A Novel High-Efficiency Parallel-Winding Connection for a Three-Phase Induction Motor Fed by a Single-Phase Power Supply", *IEEE Transactions on Energy Conversion*, vol. 29, no. 2, pp. 269–277, 2014, doi:10.1109/TEC.2014.2305755.

[4] Y. Huangfu, S. Wang, J. Qiu, H. Zhang, G. Wang, J. Zhu, "Transient Performance Analysis of Induction Motor Using Field-Circuit Coupled Finite-Element Method", *IEEE Transactions on Magnetics*, vol. 50, no. 2, pp. 873–876, 2014, doi:10.1109/TMAG.2013.2281314.

[5] W. T. Thomson, M. Fenger, "Current signature analysis to detect induction motor faults", *IEEE Industry Applications Magazine*, vol. 7, no. 4, pp. 26–34, 2001, doi:10.1109/2943.930988.

[6] A. Siddique, G. S. Yadava, B. Singh, "A review of stator fault monitoring techniques of induction motors", *IEEE Transactions on Energy Conversion*, vol. 20, no. 1, pp. 106–114, 2005, doi:10.1109/TEC.2004.837304.

[7] D. López-Pérez, J. Antonino-Daviu, "Application of Infrared Thermography to Failure Detection in Industrial Induction Motors: Case Stories", *IEEE Transactions on Industry Applications*, vol. 53, no. 3, pp. 1901–1908, 2017, doi:10.1109/TIA.2017.2655008.

[8] S. E. Pandarakone, Y. Mizuno, H. Nakamura, "Distinct Fault Analysis of Induction Motor Bearing Using Frequency Spectrum Determination and Support Vector Machine", *IEEE Transactions on Industry Applications*, vol. 53, no. 3, pp. 3049–3056, 2017, doi:10.1109/TIA.2016.2639453.

[9] J. Pons-Llinares, J. A. Antonino-Daviu, M. Riera-Guasp, S. Bin Lee, T. Kang, C. Yang, "Advanced Induction Motor Rotor Fault Diagnosis Via Continuous and Discrete Time–Frequency Tools", *IEEE Transactions on Industrial Electronics*, vol. 62, no. 3, pp. 1791–1802, 2015, doi:10.1109/TIE.2014.2355816.

[10] M. Garcia, P. A. Panagiotou, J. A. Antonino-Daviu, K. N. Gyftakis, "Efficiency Assessment of Induction Motors Operating Under Different Faulty Conditions", *IEEE Transactions on Industrial Electronics*, vol. 66, no. 10, pp. 8072–8081, 2019, doi:10.1109/TIE.2018.2885719.

[11] S. Choi, E. Pazouki, J. Baek, H. R. Bahrami, "Iterative Condition Monitoring and Fault Diagnosis Scheme of Electric Motor for Harsh Industrial Application", *IEEE Transactions on Industrial Electronics*, vol. 62, no. 3, pp. 1760–1769, 2015, doi:10.1109/TIE.2014.2361112.

[12] F. J. T. E. Ferreira, G. Baoming, A. T. de Almeida, "Reliability and Operation of High-Efficiency Induction Motors", *IEEE Transactions on Industry Applications*, vol. 52, no. 6, pp. 4628–4637, 2016, doi:10.1109/TIA.2016.2600677.

[13] E. J. Wiedenbrug, A. Ramme, E. Matheson, A. von Jouanne, A. K. Wallace, "Modern online testing of induction motors for predictive maintenance and monitoring", *IEEE Transactions on Industry Applications*, vol. 38, no. 5, pp. 1466–1472, 2002, doi:10.1109/TIA.2002.802992.

[14] M. M. O'Kane, M. J. Sander, "Intelligent motors move to the forefront of predictive maintenance", *IEEE Industry Applications Magazine*, vol. 6, no. 5, pp. 47–51, 2000, doi:10.1109/2943.863635.

[15] B. Lu, D. B. Durocher, P. Stemper, "Predictive maintenance techniques", *IEEE Industry Applications Magazine*, vol. 15, no. 6, pp. 52–60, 2009, doi:10.1109/MIAS.2009.934444.

[16] H. Behbahanifard, H. Karshenas, A. Sadoughi, "Non-invasive on-line detection of winding faults in induction motors—A review", *in 2008 International Conference on Condition Monitoring and Diagnosis*, pp. 188–191, 2008, doi:10.1109/CMD.2008.4580260.

[17] X. Liang, "Temperature Estimation and Vibration Monitoring for Induction Motors and the Potential Application in Electrical Submersible Motors", *Canadian Journal of Electrical and Computer Engineering*, vol. 42, no. 3, pp. 148–162, 2019, doi:10.1109/CJECE.2018.2875111.

[18] A. Garcia-Perez, R. d. J. Romero-Troncoso, E. Cabal-Yepez, R. A. Osornio-Rios, "The Application of High-Resolution Spectral Analysis for Identifying Multiple Combined Faults in Induction Motors", *IEEE Transactions on Industrial Electronics*, vol. 58, no. 5, pp. 2002–2010, 2011, doi:10.1109/TIE.2010.2051398.

[19] X. Liang, M. Z. Ali, H. Zhang, "Induction Motors Fault Diagnosis Using Finite Element Method: A Review", *IEEE Transactions on Industry Applications*, vol. 56, no. 2, pp. 1205–1217, 2020, doi:10.1109/TIA.2019.2958908.

[20] M. Moghadasian, S. M. Shakouhi, S. S. Moosavi, "Induction motor fault diagnosis using ANFIS based on vibration signal spectrum analysis", *in 2017 3rd International Conference on Frontiers of Signal Processing (ICFSP)*, pp. 105–108, 2017, doi:10.1109/ICFSP.2017.8097151.

[21] G. Betta, C. Liguori, A. Paolillo, A. Pietrosanto, "A DSP-based FFT-analyzer for the fault diagnosis of rotating machine based on vibration analysis", *IEEE Transactions on Instrumentation and Measurement*, vol. 51, no. 6, pp. 1316–1322, 2002, doi:10.1109/TIM.2002.807987.

[22] H. Henao, G. Capolino, M. Fernandez-Cabanas, F. Filippetti, C. Bruzzese, E. Strangas, R. Pusca, J. Estima, M. Riera-Guasp, S. Hedayati-Kia, "Trends in Fault Diagnosis for Electrical Machines: A Review of Diagnostic Techniques", *IEEE Industrial Electronics Magazine*, vol. 8, no. 2, pp. 31–42, 2014, doi:10.1109/MIE.2013.2287651.

[23] A. A. Oliveira, J. R. B. de A. Monteiro, M. L. Aguiar, D. P. Gonzaga, "Extended DQ Transformation for Vectorial Control Applications of Non-sinusoidal Permanent Magnet AC Machines", *in 2005 IEEE 36th Power Electronics Specialists Conference*, pp. 1807–1812, 2005, doi:10.1109/PESC.2005.1581876.

[24] S. Cruz, A. Cardoso, "Rotor cage fault diagnosis in three-phase induction motors, by Extended Park's Vector Approach", *Electric Machines and Power Systems*, vol. 28, pp. 289–299, 04 2000, doi:10.1080/073135600268261.

[25] C. Sun, M. Ma, Z. Zhao, X. Chen, "Sparse Deep Stacking Network for Fault Diagnosis of Motor", *IEEE Transactions on Industrial Informatics*, vol. 14, no. 7, pp. 3261–3270, 2018, doi:10.1109/TII.2018.2819674.

[26] M. Gan, C. Wang, C. Zhu, "Construction of hierarchical diagnosis network based on deep learning and its application in the fault pattern recognition of rolling element bearings", *Mechanical Systems and Signal Processing*, vol. 72-73, 11 2015, doi:10.1016/j.ymssp.2015.11.014.

[27] C. Morales-Perez, J. Rangel-Magdaleno, H. Peregrina-Barreto, J. P. Amezquita-Sanchez, M. Valtierra-Rodriguez, "Incipient Broken Rotor Bar Detection in Induction Motors Using Vibration Signals and the Orthogonal Matching Pursuit Algorithm", *IEEE Transactions on Instrumentation and Measurement*, vol. 67, no. 9, pp. 2058–2068, 2018, doi:10.1109/TIM.2018.2813820.

[28] B. R. Nayana, P. Geethanjali, "Analysis of Statistical Time-Domain Features Effectiveness in Identification of Bearing Faults From Vibration Signal", *IEEE Sensors Journal*, vol. 17, no. 17, pp. 5618–5625, 2017, doi:10.1109/JSEN.2017.2727638.

[29] J. J. Saucedo-Dorantes, M. Delgado-Prieto, R. A. Osornio-Rios, R. de Jesus Romero-Troncoso, "Multifault Diagnosis Method Applied to an Electric Machine Based on High-Dimensional Feature Reduction", *IEEE Transactions on Industry Applications*, vol. 53, no. 3, pp. 3086–3097, 2017, doi:10.1109/TIA.2016.2637307.

BIOGRAPHIES

Daniel P. Sifuentes Filho received the B.Sc degree in electrical engineering from the School of Electrical, Mechanical and Computing Engineering, Federal University of Goiás, Goiânia.

Ygor F. Ginu received the B.Sc degree in electrical engineering from the School of Electrical, Mechanical and Computing Engineering, Federal University of Goiás, the B.Sc degree in Mechanical Engineering from Paulista University (UNIP) and the M.Sc degree in Production Engineering from Federal University of Goiás, Goiânia.

Khristian M. de Andrade Jr received the B.Sc. and M.Sc. degrees in electrical engineering from the Federal University of Goiás, Goiânia, Brazil, where he is currently pursuing the Ph.D. degree.

Bernardo P. de Alvarenga received the B.E. degree from the University of Brasília, Brazil, the M.Sc. degree from the Federal University of Uberlândia, Brazil, and the Ph.D. degree from the University of São Paulo, Brazil, all in electrical engineering. He is currently a Professor with the Federal University of Goiás, Goiânia, Brazil.

Geyverson T. de Paula received the B.E., M.Sc., and Ph.D. degrees in electrical engineering from the University of São Paulo, São Carlos, Brazil.

He is currently a Professor with the Federal University of Goiás, Goiânia, Brazil.